

# DreamPhysics: Learning Physics-Based 3D Dynamics with Video Diffusion Priors

Tianyu Huang<sup>1,2</sup> Haoze Zhang<sup>2</sup> Yihan Zeng<sup>3</sup> Zhilu Zhang<sup>2</sup>  
Hui Li<sup>2</sup> Wangmeng Zuo<sup>2</sup> Rynson W. H. Lau<sup>1</sup>

<sup>1</sup>City University of Hong Kong <sup>2</sup>Harbin Institute of Technology <sup>3</sup>Huawei Noah's Ark Lab

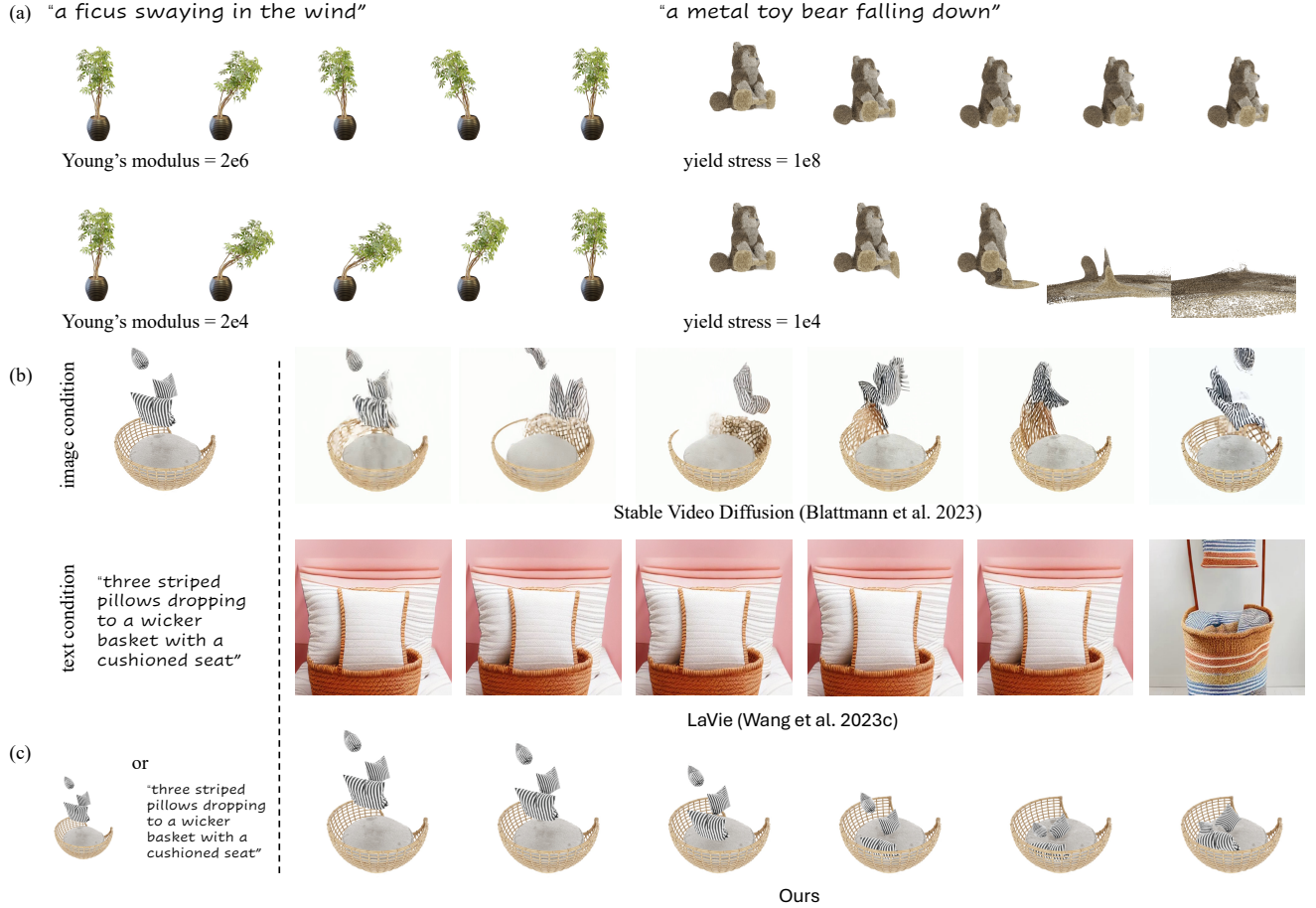


Figure 1: (a): The values of physical properties can significantly affect the quality of the simulated videos. (b) Using state-of-the-art video diffusion models (Blattmann et al. 2023; Wang et al. 2023c) can hardly generate the desired results. (c) Our DreamPhysics can produce realistic 3D dynamic content with the distillation of video diffusion priors.

## Abstract

Dynamic 3D interaction has been attracting a lot of attention recently. However, creating such 4D content remains challenging. One solution is to animate 3D scenes with physics-based simulation, which requires manually assigning precise physical properties to the object or the simulated results would become unnatural. Another solution is to learn the deformation of 3D objects with the distillation of video generative models, which, however, tends to produce 3D videos with small and discontinuous motions due to the inappropriate extraction and application of physical prior. In this work,

combining the strengths and complementing shortcomings of the above two solutions, we propose to learn the physical properties of a material field with video diffusion priors, and then utilize a physics-based Material-Point-Method (MPM) simulator to generate 4D content with realistic motions. In particular, we propose motion distillation sampling to emphasize video motion information during distillation. Moreover, to facilitate the optimization, we further propose a KAN-based material field with frame boosting. Experimental results demonstrate that our method enjoys more realistic motion than state-of-the-arts. Codes are released at: <https://github.com/tyhuang0428/DreamPhysics>.

## Introduction

With the development in 3D representation, *e.g.*, Neural Radiance Fields (NeRF) (Mildenhall et al. 2021) and 3D Gaussian Splatting (GS) (Kerbl et al. 2023), significant progress has been made in creating 3D assets through reconstruction and generation (Poole et al. 2022; Wang et al. 2024). However, interacting with these 3D assets in a simulation environment (Savva et al. 2019; Xia et al. 2018) remains challenging, while it is critical in various applications, *e.g.*, video games (Fan et al. 2022), virtual reality (Jiang et al. 2024), and robotic manipulation (Lu et al. 2024).

Animating static 3D objects based on instructions is an important step toward this interaction goal. In the physical world, object movement is intertwined with the object’s internal properties (*e.g.*, material types). Hence, we can see that on the one hand, some works (Xie et al. 2023; Feng et al. 2024b) first inject physical parameters into 3D GS objects, and then perform motion predictions in a physics-based simulator. However, as all these parameters have to be manually assigned, it is difficult to set them accurately, thus producing unnatural simulation results, as demonstrated in Figure 1(a). On the other hand, pre-trained video generators (Singer et al. 2022; Khachatryan et al. 2023; Wang et al. 2023b) have been trained with real-world video data that naturally considers physical phenomena and regulations. These generators should contain, to some extent, physics-based prior knowledge. Thus, some works (Singer et al. 2023; Bahmani et al. 2023; Zhao et al. 2023b) directly learn time-dependent deformation with the distillation of video diffusion models. However, the generated motions tend to present small and discontinuous motions across frames. We hypothesize that the main reason for this is the inappropriate extraction and application of the physical prior, rather than the utilization of video models. We therefore ask this question: how can we mine and apply the physical knowledge of the video generative models to achieve realistic dynamic 3D synthesis?

To this end, we rethink the usage of physics-based simulation and video generative models in this work. We propose to learn a material field, rather than a deformation field, from video diffusion models, and then deploy a physics-based simulator to animate the 3D object in this field. As such, the advantages of the above two related approaches are combined, while their shortcomings can be complemented. Learnable physical properties from video diffusion models eliminate the need for manual modulation, and the physical simulator based on reasonable properties ensures more realistic motion generation.

Specifically, we introduce a new framework named DreamPhysics. DreamPhysics takes 3D GS (Kerbl et al. 2023) as a 3D representation. It first learns the physical properties of a material field with the distillation of video diffusion priors, and then adopts a simulator based on Material Point Method (MPM) (Stomakhin et al. 2013; Jiang et al. 2016) to model the time-dependent deformation of each Gaussian kernel. During distillation from video diffusion models, common Score Distillation Sampling (SDS) (Poole et al. 2022) may focus more on color information and is not completely suitable for extracting motion information. Instead, we propose motion distillation sampling (MDS) to

avoid the interference of color bias and emphasize the motion information in the rendered video. In addition, directly optimizing the material field can easily lead to unstable training due to the large range of possible parameter values. To facilitate the training process, we propose a KAN-based (Liu et al. 2024) material field with frame boosting.

We note that there is a concurrent work named PhysDreamer (Zhang et al. 2024), which supervises the prediction of physical properties with a ground-truth video generated by an image-to-video diffusion model. However, as shown in Figure 1(b), the video generative model can hardly produce the desired results to serve as ground truth, due to its poor motion control over the image/text condition. In contrast, our DreamPhysics supports both image-conditioned and text-conditioned optimization without the need for pre-generated ground truth, as demonstrated in Figure 1(c). Experimental results demonstrate that our method can effectively distill the video diffusion prior and assign proper values to the physical properties. Compared with state-of-the-art works, our results enjoy more realistic motion.

Our main contributions can be summarized as:

- We introduce a physics-based 3D animation framework, *i.e.*, DreamPhysics, which learns a material field for a physical simulator to support the creation of dynamic 3D content.
- We propose motion distillation sampling for the optimization of physical properties with video diffusion priors. To facilitate the optimization, we further propose a KAN-based material field with frame boosting.
- DreamPhysics can generate high-quality 4D content with either image- or text-conditioned optimization. Extensive experiments show that our results enjoy more realistic motion simulation.

## Related Work

### 3D Generation

In recent years, 3D generation has advanced significantly, with methods broadly classified into two main categories: 3D supervised and 2D lifting approaches.

3D supervised methods (Nichol et al. 2022; Cheng et al. 2023; Wei et al. 2023; Jun and Nichol 2023; Yu et al. 2023; Huang et al. 2023b; Hong et al. 2023; Tang et al. 2024) utilize text-3D data to train generators capable of directly producing 3D assets. For instance, Point-E (Nichol et al. 2022) is an early example of a text-to-3D generator that creates point clouds based on input prompts. Shap-E (Jun and Nichol 2023) and LGM (Tang et al. 2024) have expanded the scope of generated content to include SDF (Park et al. 2019) and 3DGS (Kerbl et al. 2023) representations, respectively. Despite their efficiency in generating solid 3D content, these methods are significantly limited by the availability of 3D data. The current scale of 3D training datasets (Reizenstein et al. 2021; Deitke et al. 2023, 2024) is much smaller compared to 2D or video datasets, resulting in a constrained open-world capability relative to image or video generators. TextField3D (Huang et al. 2023b) attempts to enhance text control in 3D generators using a noisy latent space, yet it

still falls short of achieving the imaginative capabilities seen in 2D generators.

Conversely, 2D lifting methods (Poole et al. 2022; Lin et al. 2023; Metzger et al. 2023; Chen et al. 2023; Wang et al. 2024) leverage the extensive prior knowledge embedded in 2D diffusion models to optimize 3D representations. DreamFusion (Poole et al. 2022) pioneered the concept of score distillation sampling (SDS), which distills 3D renderings into 2D diffusion. Although these methods produce photo-realistic results, they are prone to 3D inconsistency issues, commonly referred to as the Janus problem.

To address this issue, recent works (Liu et al. 2023a; Zhao et al. 2023a; Shi et al. 2023; Liu et al. 2023b; Long et al. 2023) have explored the synthesis of multi-view images of 3D objects. For example, Zero-1-to-3 (Liu et al. 2023a) generates images of the same object from different viewpoints based on a given image and viewpoint angles. MVDream (Shi et al. 2023) enhances consistency by generating orthogonal multi-view images of the same object. Wonder3D (Long et al. 2023) supports depth generation to achieve more precise object reconstruction.

In this work, we collect static 3D scenes from both reconstruction data and 3D generation methods, providing more available assets for evaluation.

### 3D Animation

3D animation creation has significantly increased demand across various applications, such as video games, virtual reality, and robotic simulation. However, manually creating such 4D content is a time-consuming process that necessitates a high level of expertise. To animate a 3D object, the common practice is to bind the object with a template skeleton, also known as rigging. TADA (Liao et al. 2023) produces 3D assets based on SMPL-X (Pavlakos et al. 2019), which is a human-body 3D template that supports animation. DreamControl (Huang et al. 2024a) proposes to generate 3D assets conditioned by input skeletons, which can be rigged easily for animation.

As the success of video generative models, some methods (Zhao et al. 2023b) attempt to leverage video diffusion models to guide the prediction of the 3D deformation. DreamGaussian4D (Ren et al. 2023) uses a pre-generated video to supervise the deformation of static scenes. Animate124 (Zhao et al. 2023b) proposes to distill the priors of video diffusion models to its deformation fields.

The deformation prediction in these methods is not accurate. Recent works (Xie et al. 2023; Feng et al. 2024a; Zhang et al. 2024) introduce physics simulation to the 3D deformation. PhysGaussian (Xie et al. 2023) deploys the finite element method to model the deformation of elastic objects like collision and shaking. Feng et al. further supports the simulation of liquid. However, these methods require manually setting the physical properties for objects before simulation. PhysDreamer (Zhang et al. 2024) attempts to optimize these properties with pre-generated videos, but the quality of generated videos can hardly be ensured. In this work, we propose to distill the priors of video diffusion models to simulation environments, enabling the automatic setting of physical properties.

## Preliminaries

### Point-Based Representation

Point cloud (Guo et al. 2020) is an explicit 3D representation, which generally consists of the coordinates for all points. Normal and color information (Dai et al. 2017; Qi et al. 2017) can also be considered to further enrich the feature space of point cloud. Despite the succinct representation, its rendering quality is heavily restricted by the number of points (Zhang et al. 2022; Huang et al. 2023a). Derived from NeRF (Mildenhall et al. 2021), 3D Gaussian Splatting (GS) (Kerbl et al. 2023) introduced a point-based explicit radiance field. Points are modeled as a set of Gaussian kernels  $\{\mathcal{G}_i\} = \{x_i, \sigma_i, \Sigma_i, C_i\}$ , where  $x_i$ ,  $\sigma_i$ ,  $\Sigma_i$ , and  $C_i$  denote the center coordinate, opacity, covariance matrix, and spherical harmonic coefficient of the  $i$ -th kernel  $\mathcal{G}_i$ . To render a 3D GS scene at a specific viewpoint  $\mathbf{r}$ , the color can be formulated as,

$$\mathbf{C} = \sum_{i=1}^N T_i \alpha_i C_i, \text{ with } T_i = \prod_{j=1}^{i-1} (1 - \alpha_j), \quad (1)$$

where  $N$  is the set of sorted Gaussian kernels related to the pixel and the viewpoint.  $\alpha_i$  is the effective opacity given by evaluating a 2D Gaussian with  $\Sigma$  and  $\sigma$ . 3D GS can reconstruct high-fidelity views by real-time rendering, and support explicit interaction and editing.

### Material Point Method

The material point method (MPM) (Zong et al. 2023) is a numerical simulation mechanic for the analysis of continuum forces. In MPM, the continuum is represented by a set of particles placed in a grid-based space. Different from mesh-based numerical mechanics, MPM can be naturally applied to point-based representation 3D GS. Following PhysGaussian (Xie et al. 2023), we have a time-dependent state for each Gaussian kernel as:

$$x_i(t) = \Delta(x_i, t), \Sigma_i(t) = F_i(t) \Sigma_i F_i(t)^T, \quad (2)$$

where  $\Delta(\cdot, t)$  and  $F_i(t)$  are the coordinate deformation and the deformation gradient at timestep  $t$ . Considering the continuum rotation  $\Omega_i(t)$ , the rendering viewpoint also requires adjustment to satisfy the view direction of spherical harmonic coefficient  $C_i$ .

### Score Distillation Sampling

The score distillation sampling (SDS) (Poole et al. 2022; Wang et al. 2023a) distills pre-trained 2D diffusion models to the parameters of 3D representation, widely used in 3D generation methods. Recently, SDS has had various extensions. Variational score Distillation (VSD) (Wang et al. 2024) proposes an additional LoRA term  $\epsilon_\theta$  to learn the distribution of current 3D scenes, which is attached to the score as,

$$\nabla_\theta \mathcal{L}_{\text{VSD}}(\theta) \triangleq \mathbb{E} \left[ \omega(t) (\hat{\epsilon}_{2\text{D}}(\mathbf{x}_t, t, y) - \hat{\epsilon}_\theta(\mathbf{x}_t, t, c, y)) \frac{\partial \mathbf{x}}{\partial \theta} \right], \quad (3)$$

where  $t$  is the noise timestep and  $y$  is the input condition.  $\hat{\epsilon}_{2\text{D}}$  and  $\hat{\epsilon}_\theta$  are noises predicted by a pre-trained 2D diffusion model and the LoRA. Another extension, SDS-T, is

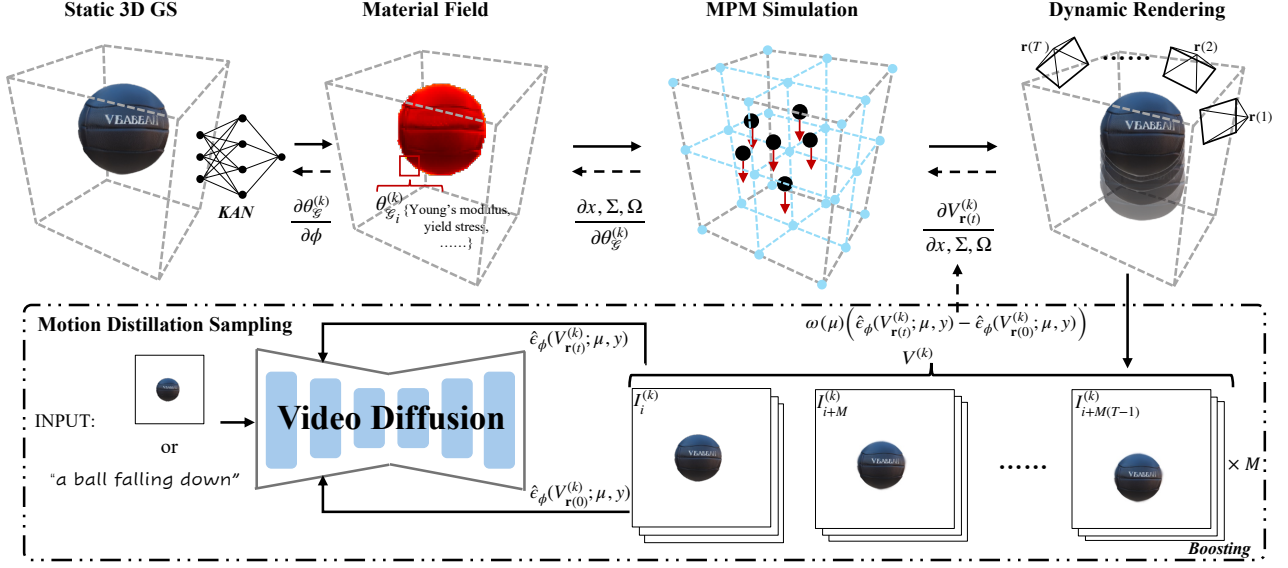


Figure 2: Overview of DreamPhysics. First, a set of physical parameters is initialized with a KAN-based (Liu et al. 2024) material field for a static 3D GS (Kerbl et al. 2023). Then, it is fed to an MPM simulator to render a 3D video. Finally, we leverage motion distillation sampling to optimize the rendered video, and the distillation gradients are back-propagated to refine the physical parameters.

for dynamic 3D generation, where video diffusion models are deployed to supervise the time-dependent deformation of static 3D objects. Specifically, given a camera trajectory  $\mathbf{r}(t)$ , SDS-T optimizes the rendered 3D video  $V_{\mathbf{r}(t)}$  with predicted noise  $\hat{\epsilon}_V$ ,

$$\nabla_{\theta} \mathcal{L}_{\text{SDS-T}}(\theta) \triangleq \mathbb{E} \left[ \omega(\mu) (\hat{\epsilon}_V(V_{\mathbf{r}(t)}; \mu, y) - \epsilon) \frac{\partial V_{\mathbf{r}(t)}}{\partial \theta} \right], \quad (4)$$

where  $\mu$  is noise timestep and  $\theta$  is target deformation.

## DreamPhysics

### Method Overview

As shown in Figure 2, given a generated object or a reconstructed scene  $\{\mathcal{G}_i\}$  represented by 3D GS (Kerbl et al. 2023), DreamPhysics aims to estimate the corresponding physical parameters  $\{\theta_{\mathcal{G}_i}\}$  for the MPM-based simulator. For each Gaussian kernel  $\mathcal{G}_i$ , we initialize its parameters  $\theta_{\mathcal{G}_i}^{(0)} = \phi(x_i)$  with a KAN-based (Liu et al. 2024) material field  $\phi$  and then simulate a time-dependent state  $\{x_i(t), \Sigma_i(t), \Omega_i(t)\}$ , which can be rendered as a  $L$ -length video  $V^{(0)} = \{I_1^{(0)}, I_2^{(0)}, \dots, I_L^{(0)}\}$ . The rendered video may look unrealistic due to the inaccurate initialization of  $\theta_{\mathcal{G}_i}^{(0)}$ . Therefore, we propose motion distillation sampling (MDS), which distills video diffusion’s motion priors while weakening its color bias. The distillation gradient is then propagated backward to the material field, updating corresponding parameters to  $\theta_{\mathcal{G}_i}^{(1)}$ . Similarly, for each training iteration  $k$ , we can obtain an optimized  $\theta_{\mathcal{G}_i}^{(k+1)}$  via the distillation of  $V^{(k)}$ . Considering current video diffusion models’ low frame rate, we further propose a frame-boosting strategy to supervise

more simulation frames. After several rounds of optimization, the final physical parameters  $\hat{\theta}_{\mathcal{G}}$  can converge to a reasonable range.

### Parameter Optimization with MDS

Video generative models are trained with real-world captured videos that cover kinds of physical phenomena. As a result, given a simulated video  $V$ , we can assess whether it adheres to physical laws based on the judgement of video models. To this end, one direct solution is to treat videos generated by video models as ground truth, supervising  $V$  with reconstruction loss (Zhang et al. 2024). However, limited by the control capability, existing video generators can hardly produce desired ground-truth videos. We consider exploring distillation methods to optimize simulated results. Motion distillation sample is thus proposed to enhance the distillation of video diffusion’s motion priors.

**Motion Distillation Sample.** With the simulation of MPM, a time-dependent state  $\{x_i(t), \Sigma_i(t), \Omega_i(t)\}$  is predicted according to Eq. (2), representing a motion in the 3D space. Our intention is to optimize this simulated motion. However, the information of a video can be divided into two terms, *i.e.*, color and motion, where color biases between video diffusion models and the simulated video should be dismissed. In VSD (Wang et al. 2024), a LoRA term pushes the distribution of the target object away from the gradient direction of the current state. Similarly, we can adopt an additional term to omit the information in the color space. We suppose that the first frame can represent the color for a whole video, so our motion distillation sample  $s_{\text{MDS}}$  is formulated as,

$$s_{\text{MDS}} = \omega(\mu) (\hat{\epsilon}_V(V_{\mathbf{r}(t)}; \mu, y) - \hat{\epsilon}_V(V_{\mathbf{r}(0)}; \mu, y)), \quad (5)$$

where  $\mathbf{r}(0)$  is the camera viewpoint in the first frame.

Note that the gradient of  $s_{\text{MDS}}$  cannot be directly propagated to the target physical parameters  $\theta_G$ , and it needs to go through the differentiable MPM. Thus, our training objective can be written as,

$$\nabla_{\theta_G} \mathcal{L}_{\text{MDS}}(\theta_G, \mathbf{r}(t)) \triangleq \mathbb{E} \left[ s_{\text{MDS}} \frac{\partial V_{\mathbf{r}(t)}}{\partial x, \Sigma, \Omega} \frac{\partial x, \Sigma, \Omega}{\partial \theta_G} \right]. \quad (6)$$

### Parameter Estimation with Material Field

The value range for physical properties  $\theta_G$  can be very large, e.g., the reasonable values for Young’s modulus can vary from 1 to  $1e7$ . However, during gradient updates, the same gradient can result in varying update granularity across different magnitudes, causing parameters to get stuck within a specific magnitude range. To enable parameters to converge more quickly to a reasonable range, we propose to perform a KAN-based tri-plane representation to model the material field and conduct frame boosting to further facilitate the training process.

**KAN-Based Triplane.** Tri-plane is widely used to encode spatial information. Given a 3D coordinate  $x$ , the tri-plane extractor projects it onto three orthogonal planes, i.e., the front view, side view, and top view. These projections match  $x$  with 2D features that represent different perspectives of the 3D space. We extract features with KAN (Liu et al. 2024), which integrates kernel methods and attention mechanisms to offer superior modeling capabilities for physics-based tasks compared to traditional MLPs. Extracted features are then combined to form a unified representation, which constitutes our physical parameters  $\theta_G$ . The gradient is propagated as,

$$\nabla_{\phi} \mathcal{L}_{\phi}(x, \mathbf{r}(t)) \triangleq \mathbb{E} \left[ \mathcal{L}_{\text{MDS}}(\phi(x), \mathbf{r}(t)) \frac{\partial \theta_G}{\partial \phi} \right]. \quad (7)$$

**Frame Boosting.** The MPM simulator is a sequential model, which can easily lead to gradient vanishing or exploding like RNN (Rumelhart, Hinton, and Williams 1986). We have to conduct truncated back-propagation through time (BPTT), preserving the gradient of key frame simulation only. Truncated BPTT can effectively prevent gradient issues, but the supervision could be limited to specific frames. To ensure that our supervision covers as many video frames as possible, we further suggest a frame-boosting strategy. Specifically, given a total number of frames  $M \times T$ , we can separate them into  $M$  groups of frames with equal intervals, i.e.,  $V_{t_i} = \{I_i, I_{i+M}, \dots, I_{i+M(T-1)}\}$  for the  $i$ -th group. These groups formulate different videos, which are fed into the supervision process alternately. Finally, the boosted motion distillation can be formulated as,

$$\mathcal{L}_{\hat{\phi}}(x) = \frac{1}{M} \sum_{i=1}^M \mathcal{L}_{\phi}(x, \mathbf{r}(t_i)), \quad (8)$$

where  $\hat{\phi}$  is the boosted material field.

## Experiments

In this section, we show our 4D generation content on both text-conditioned and image-conditioned optimizations and

compare it with previous state-of-the-art methods. Extensive ablation studies are then conducted to demonstrate the effectiveness of our newly proposed components.

### Experimental Setup

**Implementation Details.** The simulation is based on the warp (Macklin 2022) implementation of MPM (Zong et al. 2023). For most simulation scenes, we set the simulation duration as  $5 \times 10^{-5}$  second and the frame duration as  $4 \times 10^{-2}$  second. Thus, we simulate 800 steps between every two renderings and include the simulation gradient of the last step in the optimization. We leverage a text-to-video diffusion model ModelScope (Wang et al. 2023b) and an image-to-video diffusion model Stable Video Diffusion (SVD) (Blattmann et al. 2023) to conduct text-conditioned and image-conditioned optimization, respectively. The numbers of their generated video frames  $T$  are 16 and 25, respectively. For frame boosting, we set  $M = 5$ , boosting the video slices to 5 groups. The setting of MDS follows SDS, where CFG value is set to 100. We stop the training if optimized parameter values stabilize within one order of magnitude. The training process requires around 30 iterations. The iteration time highly depends on the number of input Gaussian kernels, and it is within 30 seconds for most cases.

**Dataset.** We collect seven 3D static scenes or objects from previous works (Xie et al. 2023; Zhang et al. 2024) and 3D GS generative models (Tang et al. 2024). The content includes three plants, a beanie hat, a telephone cord, a sofa with pillows, and a ball, where two motions (rotation and collision) are involved in the simulator.

**Evaluation Metric.** We use the aesthetic quality from VBench (Huang et al. 2024b), grading the artistic score from 0 to 10 using the LAION aesthetic predictor (LAION-AI 2022). This metric can reflect aesthetic aspects such as the naturalness of the video, which exactly meets our evaluation requirements. In addition, we will add user study results in the supplementary materials.

**Compared Methods.** Since physics-based 4D generation is still under development, we compare three existing methods PhysGaussian (Xie et al. 2023), PhysDreamer (Zhang et al. 2024), and DreamGaussian4D (Ren et al. 2023). PhysGaussian is a pioneer work that manually sets all the physical properties in a physics-based simulator. PhysDreamer is a concurrent work that supervises physical parameters with ground-truth videos. DreamGaussian4D predicts the deformation of 3D GS without physical constraint, which is different from the above two works.

### 3D Dynamics Generation

**Text Condition.** In Figure 3(a), we select the ficus scene in PhysGaussian (Xie et al. 2023) and input a text prompt “*ficus swaying in the wind*” to simulate the rotation motion. The ficus would excessively tilt to one side and have difficulty returning to its original position if its Young’s modulus is set too low. After the optimization by our DreamPhysics, Young’s modulus falls within a normal range, and the swaying looks more natural. From the space-time slices, the optimized motion trajectory looks more realistic.



Figure 3: (a) Text-conditioned optimization. The ficus will excessively tilt to one side before optimization; (b) Image-conditioned optimization. Right images are the space-time (X-t) slices, one axis represents time and the other axis shows a space slice (red line) of the object.

Table 1: Quantitative results for the comparison with previous works on 4 scenes from Figure 4. The higher aesthetic quality score indicates better generation quality.

DreamGaussian4D	PhysGaussian	PhysDreamer	Ours	GT
4.61	4.98	4.84	<b>5.03</b>	5.13

**Image Condition.** For image-conditioned optimization, the first frame is regarded as the input image. We select a generated ball and try to optimize its dropping process, which is an example of collision motion, as shown in Figure 3(b). When hitting the ground, the ball would exhibit excessive deformation if the physical properties are not initialized accurately. Our method can effectively adjust these properties to a reasonable range after the optimization.

**Comparison with State-of-the-art Works.** We report the quantitative results of all the compared methods in Table 1. Since PhysDreamer hasn’t released its training implementation, we can only compare four evaluation scenes, which are provided in PhysDreamer’s video demo. Considering that other methods don’t have extra text inputs, we use the first frame as the image condition to conduct the optimization. According to the evaluation of aesthetic quality, our results are the closest to the ground truth. PhysDreamer has a lower score compared with PhysGaussian, which indicates that pre-generated videos may not be a proper ground truth for supervision. The generation quality of DreamGaussian4D is the worst because its deformation prediction didn’t consider physical constraints.

We also provide the visualization of space-time slices in Figure 4. Since all the physical properties in PhysGaussian are manually set, its generated motions often look too ex-

Table 2: Quantitative results of ablation study on 7 scenes. **Score** denotes the average aesthetic quality score, and **Iter** denotes the average training iterations.

Method	+KAN	+ $\mathcal{L}_{\text{MDS}}$	+Boost	<b>Score</b> ↑	<b>Iter</b> ↓
(a)				4.86	36.86
(b)	✓			4.89	34.29
(c)	✓	✓		<b>4.94</b>	33.86
Ours	✓	✓	✓	4.93	<b>29.71</b>

tre. DreamGaussian4D generates the most consistent motions but appears less natural, as its prediction lacks physical constraint. PhysDreamer can exhibit energy dissipation to some extent, while our results look more similar to the ground-truth visualization, in terms of amplitude and frequency of the simulated motions.

## Ablation Study

To evaluate the effectiveness of our newly proposed modules, we conduct ablation studies on all 7 scenes. Our baseline uses a vanilla SDS-T loss (Eq. (4)), where gradients are propagated to the physical parameters without KAN. Based on this, we attach our KAN-based material field, motion distillation sampling, and frame boosting step by step.

We report the aesthetic quality score and training iterations in Table 2. In (a), the physical parameters can hardly converge to a reasonable range, with the evaluation score and required iterations being the worst. Equipped with a KAN-based material field, (b) can facilitate the optimization and improve the generation quality. Then, we use motion distillation sampling  $\mathcal{L}_{\text{MDS}}$  in (c), where the aesthetic score is further improved. In (d), our final method enjoys a faster



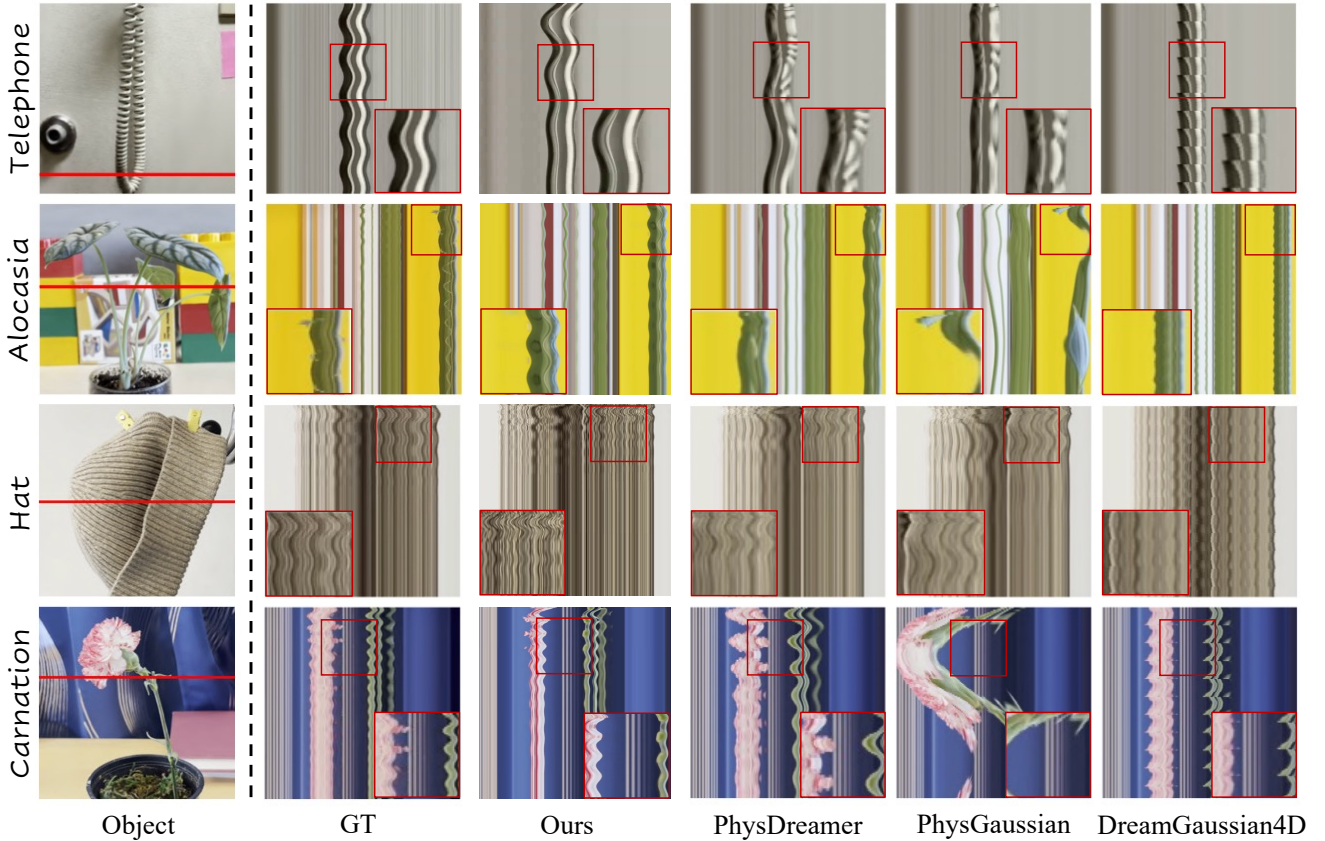


Figure 4: Visualization of space-time slices. Compared with previous works, our results are more close to the ground truth.

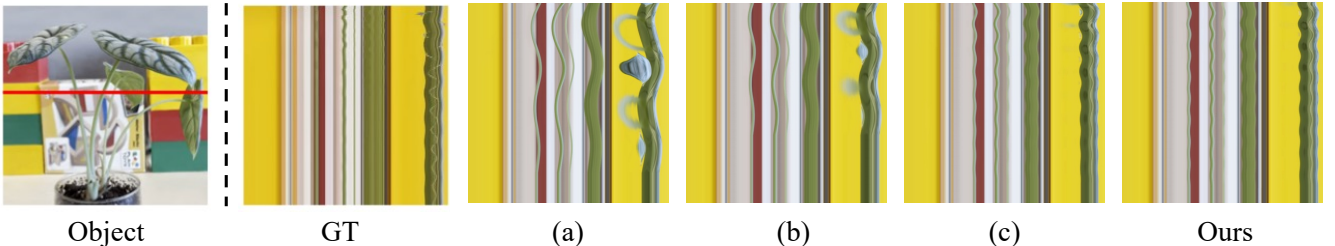


Figure 5: Visualization of space-time slices for ablation study. (a) and (b) are not quite consistent with the ground truth. (c) and our method can generate closer content compared with the ground truth.

optimization speed within 30 training iterations, demonstrating that our frame boosting can fasten the parameter convergence. Note that, frame boosting is not designed for optimization quality, so our final score is similar to (c).

We provide the visualization of the Alocasia scene in Figure 5. The space-time slices of (a) and (b) are not quite consistent with the ground truth, while (c) and our final method can produce 4D content that is competitive to real-captured videos. These results are consistent with our quantitative results in Table 2.

## Conclusion

In this work, we introduced a new framework DreamPhysics, which learns the physical properties of 3D Gaussian Splatting with video diffusion priors. Based on the physics-based simulation, DreamPhysics distills the motion priors

to physical parameters with motion distillation sampling. To facilitate that process, we further propose a KAN-based material field with frame boosting. Extensive experiments demonstrate that our method can produce high-quality 4D content with both text and image conditions.

Albeit the improvement compared with previous works, the physics-based 3D dynamics research still faces two problems, *i.e.*, simulated motions and scene-level interaction. Each kind of motion depends on independent physical constraints. Current frameworks can hardly combine all the motions into one simulator. Moreover, simulators can only handle the interactions of a few target objects, but environments are dismissed. For example, in the simulation of the telephone (Figure 4), shadows on the wall cannot change with the movement of the telephone cord. We will explore these problems for future work.

## References

- Bahmani, S.; Skorokhodov, I.; Rong, V.; Wetzstein, G.; Guibas, L.; Wonka, P.; Tulyakov, S.; Park, J. J.; Tagliasacchi, A.; and Lindell, D. B. 2023. 4d-fy: Text-to-4d generation using hybrid score distillation sampling. *arXiv preprint arXiv:2311.17984*.
- Blattmann, A.; Dockhorn, T.; Kulal, S.; Mendelevitch, D.; Kilian, M.; Lorenz, D.; Levi, Y.; English, Z.; Voleti, V.; Letts, A.; et al. 2023. Stable video diffusion: Scaling latent video diffusion models to large datasets. *arXiv preprint arXiv:2311.15127*.
- Carreira, J.; and Zisserman, A. 2017. Quo vadis, action recognition? A new model and the Kinetics dataset. In *Proceedings of the IEEE Conference on Computer Vision and Pattern Recognition (CVPR)*, 6299–6308.
- Chen, R.; Chen, Y.; Jiao, N.; and Jia, K. 2023. Fantasia3D: Disentangling Geometry and Appearance for High-quality Text-to-3D Content Creation. In *Proceedings of the IEEE/CVF International Conference on Computer Vision (ICCV)*, 22246–22256.
- Cheng, Y.-C.; Lee, H.-Y.; Tulyakov, S.; Schwing, A. G.; and Gui, L.-Y. 2023. Sdfusion: Multimodal 3d shape completion, reconstruction, and generation. In *Proceedings of the IEEE/CVF Conference on Computer Vision and Pattern Recognition*, 4456–4465.
- Dai, A.; Chang, A. X.; Savva, M.; Halber, M.; Funkhouser, T.; and Nießner, M. 2017. ScanNet: Richly-annotated 3D reconstructions of indoor scenes. In *Proceedings of the IEEE conference on computer vision and pattern recognition*, 5828–5839.
- Deitke, M.; Liu, R.; Wallingford, M.; Ngo, H.; Michel, O.; Kusupati, A.; Fan, A.; Laforte, C.; Voleti, V.; Gadre, S. Y.; et al. 2024. Objaverse-xl: A universe of 10m+ 3d objects. *Advances in Neural Information Processing Systems*, 36.
- Deitke, M.; Schwenk, D.; Salvador, J.; Weihs, L.; Michel, O.; VanderBilt, E.; Schmidt, L.; Ehsani, K.; Kembhavi, A.; and Farhadi, A. 2023. Objaverse: A universe of annotated 3d objects. In *Proceedings of the IEEE/CVF Conference on Computer Vision and Pattern Recognition*, 13142–13153.
- Fan, L.; Wang, G.; Jiang, Y.; Mandlekar, A.; Yang, Y.; Zhu, H.; Tang, A.; Huang, D.-A.; Zhu, Y.; and Anandkumar, A. 2022. Minedojo: Building open-ended embodied agents with internet-scale knowledge. *Advances in Neural Information Processing Systems*, 35: 18343–18362.
- Feng, Y.; Feng, X.; Shang, Y.; Jiang, Y.; Yu, C.; Zong, Z.; Shao, T.; Wu, H.; Zhou, K.; Jiang, C.; and Yang, Y. 2024a. Gaussian Splashing: Unified Particles for Versatile Motion Synthesis and Rendering. *arXiv preprint arXiv:2401.15318*.
- Feng, Y.; Feng, X.; Shang, Y.; Jiang, Y.; Yu, C.; Zong, Z.; Shao, T.; Wu, H.; Zhou, K.; Jiang, C.; et al. 2024b. Gaussian Splashing: Dynamic Fluid Synthesis with Gaussian Splatting. *arXiv preprint arXiv:2401.15318*.
- Guo, Y.; Wang, H.; Hu, Q.; Liu, H.; Liu, L.; and Bennamoun, M. 2020. Deep learning for 3D point clouds: A survey. *IEEE Transactions on Pattern Analysis and Machine Intelligence*.
- Heusel, M.; Ramsauer, H.; Unterthiner, T.; Nessler, B.; and Hochreiter, S. 2017. Gans trained by a two time-scale update rule converge to a local nash equilibrium. *Advances in neural information processing systems*, 30.
- Hong, Y.; Zhang, K.; Gu, J.; Bi, S.; Zhou, Y.; Liu, D.; Liu, F.; Sunkavalli, K.; Bui, T.; and Tan, H. 2023. Lrm: Large reconstruction model for single image to 3d. *arXiv preprint arXiv:2311.04400*.
- Huang, T.; Dong, B.; Yang, Y.; Huang, X.; Lau, R. W.; Ouyang, W.; and Zuo, W. 2023a. Clip2point: Transfer clip to point cloud classification with image-depth pre-training. In *Proceedings of the IEEE/CVF International Conference on Computer Vision*, 22157–22167.
- Huang, T.; Zeng, Y.; Dong, B.; Xu, H.; Xu, S.; Lau, R. W.; and Zuo, W. 2023b. TextField3D: Towards Enhancing Open-Vocabulary 3D Generation with Noisy Text Fields. *arXiv preprint arXiv:2309.17175*.
- Huang, T.; Zeng, Y.; Zhang, Z.; Xu, W.; Xu, H.; Xu, S.; Lau, R. W.; and Zuo, W. 2024a. Dreamcontrol: Control-based text-to-3d generation with 3d self-prior. In *Proceedings of the IEEE/CVF Conference on Computer Vision and Pattern Recognition*, 5364–5373.
- Huang, Z.; He, Y.; Yu, J.; Zhang, F.; Si, C.; Jiang, Y.; Zhang, Y.; Wu, T.; Jin, Q.; Chanpaisit, N.; Wang, Y.; Chen, X.; Wang, L.; Lin, D.; Qiao, Y.; and Liu, Z. 2024b. VBench: Comprehensive Benchmark Suite for Video Generative Models. In *Proceedings of the IEEE/CVF Conference on Computer Vision and Pattern Recognition*.
- Huynh-Thu, Q.; and Ghanbari, M. 2008. *The Scope of Image Quality Metrics*, volume 6806. SPIE.
- Jiang, C.; Schroeder, C.; Teran, J.; Stomakhin, A.; and Selle, A. 2016. The material point method for simulating continuum materials. In *Acm siggraph 2016 courses*, 1–52.
- Jiang, Y.; Yu, C.; Xie, T.; Li, X.; Feng, Y.; Wang, H.; Li, M.; Lau, H.; Gao, F.; Yang, Y.; et al. 2024. VR-GS: a physical dynamics-aware interactive gaussian splatting system in virtual reality. In *ACM SIGGRAPH 2024 Conference Papers*, 1–1.
- Jun, H.; and Nichol, A. 2023. Shap-E: Generating Conditional 3D Implicit Functions. *arXiv preprint arXiv:2305.02463*.
- Kerbl, B.; Kopanas, G.; Leimkühler, T.; and Drettakis, G. 2023. 3D Gaussian Splatting for Real-Time Radiance Field Rendering. *ACM Transactions on Graphics*, 42(4).
- Khachatryan, L.; Movsisyan, A.; Tadevosyan, V.; Henschel, R.; Wang, Z.; Navasardyan, S.; and Shi, H. 2023. Text2video-zero: Text-to-image diffusion models are zero-shot video generators. In *Proceedings of the IEEE/CVF International Conference on Computer Vision*, 15954–15964.
- LAION-AI. 2022. aesthetic-predictor.
- Li, Z.; Zhu, Z.-L.; Han, L.-H.; Hou, Q.; Guo, C.-L.; and Cheng, M.-M. 2023. Amt: All-pairs multi-field transforms for efficient frame interpolation. In *Proceedings of the IEEE/CVF Conference on Computer Vision and Pattern Recognition*, 9801–9810.



- Liao, T.; Yi, H.; Xiu, Y.; Tang, J.; Huang, Y.; Thies, J.; and Black, M. J. 2023. Tada! text to animatable digital avatars. *arXiv preprint arXiv:2308.10899*.
- Lin, C.-H.; Gao, J.; Tang, L.; Takikawa, T.; Zeng, X.; Huang, X.; Kreis, K.; Fidler, S.; Liu, M.-Y.; and Lin, T.-Y. 2023. Magic3d: High-resolution text-to-3d content creation. In *Proceedings of the IEEE/CVF Conference on Computer Vision and Pattern Recognition*, 300–309.
- Liu, R.; Wu, R.; Van Hoorick, B.; Tokmakov, P.; Zakharov, S.; and Vondrick, C. 2023a. Zero-1-to-3: Zero-shot one image to 3d object. In *Proceedings of the IEEE/CVF International Conference on Computer Vision*, 9298–9309.
- Liu, Y.; Lin, C.; Zeng, Z.; Long, X.; Liu, L.; Komura, T.; and Wang, W. 2023b. SyncDreamer: Generating Multiview-consistent Images from a Single-view Image. *arXiv preprint arXiv:2309.03453*.
- Liu, Z.; Wang, Y.; Vaidya, S.; Ruehle, F.; Halverson, J.; Soljačić, M.; Hou, T. Y.; and Tegmark, M. 2024. Kan: Kolmogorov-arnold networks. *arXiv preprint arXiv:2404.19756*.
- Long, X.; Guo, Y.-C.; Lin, C.; Liu, Y.; Dou, Z.; Liu, L.; Ma, Y.; Zhang, S.-H.; Habermann, M.; Theobalt, C.; et al. 2023. Wonder3D: Single Image to 3D using Cross-Domain Diffusion. *arXiv preprint arXiv:2310.15008*.
- Lu, G.; Zhang, S.; Wang, Z.; Liu, C.; Lu, J.; and Tang, Y. 2024. Manigaussian: Dynamic gaussian splatting for multi-task robotic manipulation. *arXiv preprint arXiv:2403.08321*.
- Macklin, M. 2022. Warp: A High-performance Python Framework for GPU Simulation and Graphics. <https://github.com/nvidia/warp>. NVIDIA GPU Technology Conference (GTC).
- Metzer, G.; Richardson, E.; Patashnik, O.; Giryas, R.; and Cohen-Or, D. 2023. Latent-nerf for shape-guided generation of 3d shapes and textures. In *Proceedings of the IEEE/CVF Conference on Computer Vision and Pattern Recognition*, 12663–12673.
- Mildenhall, B.; Srinivasan, P. P.; Tancik, M.; Barron, J. T.; Ramamoorthi, R.; and Ng, R. 2021. Nerf: Representing scenes as neural radiance fields for view synthesis. *Communications of the ACM*, 65(1): 99–106.
- Nichol, A.; Jun, H.; Dhariwal, P.; Mishkin, P.; and Chen, M. 2022. Point-E: A System for Generating 3D Point Clouds from Complex Prompts. *arXiv preprint arXiv:2212.08751*.
- Park, J. J.; Florence, P.; Straub, J.; Newcombe, R.; and Lovegrove, S. 2019. DeepSDF: Learning continuous signed distance functions for shape representation. In *Proceedings of the IEEE/CVF conference on computer vision and pattern recognition*, 165–174.
- Pavlakos, G.; Choutas, V.; Ghorbani, N.; Bolkart, T.; Osman, A. A.; Tzionas, D.; and Black, M. J. 2019. Expressive body capture: 3d hands, face, and body from a single image. In *Proceedings of the IEEE/CVF conference on computer vision and pattern recognition*, 10975–10985.
- Poole, B.; Jain, A.; Barron, J. T.; and Mildenhall, B. 2022. Dreamfusion: Text-to-3d using 2d diffusion. *arXiv preprint arXiv:2209.14988*.
- Qi, C. R.; Su, H.; Mo, K.; and Guibas, L. J. 2017. PointNet: Deep learning on point sets for 3D classification and segmentation. In *Proceedings of the IEEE conference on computer vision and pattern recognition*, 652–660.
- Reizenstein, J.; Shapovalov, R.; Henzler, P.; Sbordone, L.; Labatut, P.; and Novotny, D. 2021. Common objects in 3d: Large-scale learning and evaluation of real-life 3d category reconstruction. In *Proceedings of the IEEE/CVF international conference on computer vision*, 10901–10911.
- Ren, J.; Pan, L.; Tang, J.; Zhang, C.; Cao, A.; Zeng, G.; and Liu, Z. 2023. DreamGaussian4D: Generative 4D Gaussian Splatting. *arXiv preprint arXiv:2312.17142*.
- Rumelhart, D. E.; Hinton, G. E.; and Williams, R. J. 1986. Learning representations by back-propagating errors. *Nature*, 323(6088): 533–536.
- Savva, M.; Kadian, A.; Maksymets, O.; Zhao, Y.; Wijmans, E.; Jain, B.; Straub, J.; Liu, J.; Koltun, V.; Malik, J.; et al. 2019. Habitat: A platform for embodied ai research. In *Proceedings of the IEEE/CVF international conference on computer vision*, 9339–9347.
- Shi, Y.; Wang, P.; Ye, J.; Long, M.; Li, K.; and Yang, X. 2023. Mvdream: Multi-view diffusion for 3d generation. *arXiv preprint arXiv:2308.16512*.
- Singer, U.; Polyak, A.; Hayes, T.; Yin, X.; An, J.; Zhang, S.; Hu, Q.; Yang, H.; Ashual, O.; Gafni, O.; et al. 2022. Make-a-video: Text-to-video generation without text-video data. *arXiv preprint arXiv:2209.14792*.
- Singer, U.; Sheynin, S.; Polyak, A.; Ashual, O.; Makarov, I.; Kokkinos, F.; Goyal, N.; Vedaldi, A.; Parikh, D.; Johnson, J.; et al. 2023. Text-to-4d dynamic scene generation. *arXiv preprint arXiv:2301.11280*.
- Stomakhin, A.; Schroeder, C.; Chai, L.; Teran, J.; and Selle, A. 2013. A material point method for snow simulation. *ACM Transactions on Graphics (TOG)*, 32(4): 1–10.
- Tang, J.; Chen, Z.; Chen, X.; Wang, T.; Zeng, G.; and Liu, Z. 2024. Lgm: Large multi-view gaussian model for high-resolution 3d content creation. *arXiv preprint arXiv:2402.05054*.
- Unterthiner, T.; Nessler, B.; Heigold, G.; Kirschbaum, S.; Kalchbrenner, N.; Ramsauer, H.; Klambauer, G.; and Hochreiter, S. 2019. Towards qualitative evaluation of video generation models. In *Workshop on Challenges and Opportunities for AI in Financial Services: the Impact of Fairness, Explainability, Accuracy, and Privacy, NeurIPS*.
- Wang, H.; Du, X.; Li, J.; Yeh, R. A.; and Shakhnarovich, G. 2023a. Score jacobian chaining: Lifting pretrained 2d diffusion models for 3d generation. In *Proceedings of the IEEE/CVF Conference on Computer Vision and Pattern Recognition*, 12619–12629.
- Wang, J.; Yuan, H.; Chen, D.; Zhang, Y.; Wang, X.; and Zhang, S. 2023b. Modelscope text-to-video technical report. *arXiv preprint arXiv:2308.06571*.
- Wang, Y.; Chen, X.; Ma, X.; Zhou, S.; Huang, Z.; Wang, Y.; Yang, C.; He, Y.; Yu, J.; Yang, P.; et al. 2023c. Lavie: High-quality video generation with cascaded latent diffusion models. *arXiv preprint arXiv:2309.15103*.

Wang, Z.; Bovik, A. C.; Sheikh, H. R.; and Simoncelli, E. P. 2004. Image quality assessment: from error visibility to structural similarity. *IEEE Transactions on Image Processing*, 13(4): 600–612.

Wang, Z.; Lu, C.; Wang, Y.; Bao, F.; Li, C.; Su, H.; and Zhu, J. 2024. Prolificdreamer: High-fidelity and diverse text-to-3d generation with variational score distillation. *Advances in Neural Information Processing Systems*, 36.

Wei, J.; Wang, H.; Feng, J.; Lin, G.; and Yap, K.-H. 2023. TAPS3D: Text-Guided 3D Textured Shape Generation from Pseudo Supervision. In *Proceedings of the IEEE/CVF Conference on Computer Vision and Pattern Recognition*, 16805–16815.

Xia, F.; Zamir, A. R.; He, Z.; Sax, A.; Malik, J.; and Savarese, S. 2018. Gibson env: Real-world perception for embodied agents. In *Proceedings of the IEEE conference on computer vision and pattern recognition*, 9068–9079.

Xie, T.; Zong, Z.; Qiu, Y.; Li, X.; Feng, Y.; Yang, Y.; and Jiang, C. 2023. Physgaussian: Physics-integrated 3d gaussians for generative dynamics. *arXiv preprint arXiv:2311.12198*.

Yu, C.; Lu, G.; Zeng, Y.; Sun, J.; Liang, X.; Li, H.; Xu, Z.; Xu, S.; Zhang, W.; and Xu, H. 2023. Towards High-Fidelity Text-Guided 3D Face Generation and Manipulation Using only Images. In *Proceedings of the IEEE/CVF International Conference on Computer Vision*, 15326–15337.

Zhang, R.; Guo, Z.; Zhang, W.; Li, K.; Miao, X.; Cui, B.; Qiao, Y.; Gao, P.; and Li, H. 2022. Pointclip: Point cloud understanding by clip. In *Proceedings of the IEEE/CVF conference on computer vision and pattern recognition*, 8552–8562.

Zhang, R.; Isola, P.; Efros, A. A.; Shechtman, E.; and Wang, O. 2018. The Unreasonable Effectiveness of Deep Features as a Perceptual Metric. *Proceedings of the IEEE Conference on Computer Vision and Pattern Recognition (CVPR)*.

Zhang, T.; Yu, H.-X.; Wu, R.; Feng, B. Y.; Zheng, C.; Snavely, N.; Wu, J.; and Freeman, W. T. 2024. PhysDreamer: Physics-Based Interaction with 3D Objects via Video Generation. *arXiv preprint arXiv:2404.13026*.

Zhao, M.; Zhao, C.; Liang, X.; Li, L.; Zhao, Z.; Hu, Z.; Fan, C.; and Yu, X. 2023a. EfficientDreamer: High-Fidelity and Robust 3D Creation via Orthogonal-view Diffusion Prior. *arXiv preprint arXiv:2308.13223*.

Zhao, Y.; Yan, Z.; Xie, E.; Hong, L.; Li, Z.; and Lee, G. H. 2023b. Animate124: Animating one image to 4d dynamic scene. *arXiv preprint arXiv:2311.14603*.

Zong, Z.; Li, X.; Li, M.; Chiaramonte, M. M.; Matusik, W.; Grinspun, E.; Carlberg, K.; Jiang, C.; and Chen, P. Y. 2023. Neural Stress Fields for Reduced-Order Elastoplasticity and Fracture. In *SIGGRAPH Asia 2023 Conference Papers*, SA '23. New York, NY, USA: Association for Computing Machinery. ISBN 9798400703157.

## Additional Experiments

### User Study

To better assess human preferences for generated 3D videos, we conducted user studies in both SOTA comparisons and ablation experiments. For each scenario, we provided four video clips and asked the participants to select the most preferred one. The selection criteria are the realism and coherence of the generated videos. A total of 28 volunteers participated in the study, including 5 professionals from the 3D art industry.

From Table 3, our method is the most favorable one in both SOTA comparisons and ablation experiments. The results are generally consistent with the quantitative evaluation metric, *i.e.*, aesthetic quality used in the main paper.

### Ablation Study on KAN

In the tri-plane of our material field, we replace the MLP encoder with KAN (Liu et al. 2024) layers to enhance the modeling of physical parameters. We conduct an ablation study on KAN layers based on our final method, using a classic MLP encoder to extract tri-plane features, instead of KAN layers. The results show that MLP generally encounters some issues in collision scenarios. As shown in Figure 6, the ball optimized by MLP is too soft to maintain its original shape, while our method can restore it.

### Video Visualization Results

We provide generated videos in the supplementary materials. Please refer to the HTML file named “results.html” or directly check the MP4 files in the “videos” folder.

## Experimental Details

### Dataset Scenes

Seven scenes are used in our experiments. Their details are as follows.

**Alocasia.** This scene is from PhysDreamer (Zhang et al. 2024), showing an alocasia swaying on a table. The simulated motion is the rotation of an elastic object. This scene has a real-captured video as the ground truth.

**Carnation.** This scene is from PhysDreamer, showing a carnation swaying on a table. The simulated motion is the rotation of an elastic object. This scene has a real-captured video as the ground truth.

**Hat.** This scene is from PhysDreamer, where a hat hanging on a clothes hanger is swaying. The simulated motion is the rotation of an elastic object. This scene has a real-captured video as the ground truth.

**Telephone.** This scene is from PhysDreamer, showing a telephone on the wall, with its cord swaying. The simulated motion is the rotation of an elastic object. This scene has a real-captured video as the ground truth.

**Ball.** Since all the evaluation scenes in PhysDreamer are used to simulate the rotation of elastic objects, we propose a collision example where a ball drops to the ground. The ball is generated by LGM (Tang et al. 2024). We place it in a gravitational field.

**Ficus.** This scene is from PhysGaussian (Xie et al. 2023), showing a ficus swaying in the wind. The simulated motion is the rotation of an elastic object.

**Pillow.** This scene is from PhysGaussian (Xie et al. 2023), where a cushion and three pillows fall onto the sofa one after another. This simulated motion is a complicated collision motion.

### Evaluation Metrics

Traditional image evaluation metrics like SSIM (Wang et al. 2004), PSNR (Huynh-Thu and Ghanbari 2008), LPIPS (Zhang et al. 2018), and FID (Heusel et al. 2017) measure the similarity of two input images, which can hardly evaluate the motion consistency compared with the ground truth. FVD (Unterthiner et al. 2019) takes temporal information into consideration, extracting spatio-temporal features with I3D (Carreira and Zisserman 2017). However, similarly to FID, this metric also focuses on frame content, rather than motion fidelity.

A recent video benchmark VBench (Huang et al. 2024b) proposes to evaluate the temporal quality of video generation with motion smoothness. In the evaluation of motion smoothness, odd-number frames are dropped from input videos and then predicted by a frame interpolation model (Li et al. 2023). The smoothness score is related to the similarity of the original frames and predicted frames. Although its motivation is to measure the smoothness of generated motion, this metric can hardly discriminate the quality of physics-based simulation results. All the physics-based methods (PhysGaussian, PhysDreamer, and our method) can achieve over 0.99 in this metric because the simulator is capable of producing continuous motions.

Actually, our evaluation objective should be judging whether a generated motion conforms to real-world physical laws. In other words, we should assess whether the generated motion looks realistic. As a result, we use aesthetic quality in VBench, calculating the average aesthetic score of all the frames as our evaluation metric. In this way, some of the frames can get low scores if the physical parameters are set inappropriately. Furthermore, the user study can better evaluate the realism and coherence of the generated videos. We also perform user studies in Table 3.

### Code and Pseudocode

We provide codes in the supplementary materials. Please refer to the “code” folder. Here, we further provide a pseudocode in Algorithm 1.

## Theoretical Details

### Material Point Method

The material point method (MPM) is a powerful numerical technique used to simulate the behavior of continuum materials. MPM discretizes a material body into a collection of material points (often referred to as particles), each carrying properties such as mass, velocity, deformation gradient, and stress. These particles are coupled with a background computational grid, which aids in the calculation of spatial derivatives and the application of external forces.

Table 3: User studies on the comparison of state-of-the-art methods and ablation methods.

Method	<i>Alocasia</i>	<i>Carnation</i>	<i>Hat</i>	<i>Telephone</i>	<i>Ball</i>	<i>Ficus</i>	<i>Pillow</i>	Total
DreamGaussian4D	3.57%	7.14%	10.71%	7.14%	-	-	-	7.14%
PhysGaussian	21.43%	10.71%	28.57%	3.57%	-	-	-	16.07%
PhysDreamer	17.86%	35.71%	7.14%	25.00%	-	-	-	21.43%
Ours	<b>57.14%</b>	<b>46.43%</b>	<b>53.57%</b>	<b>64.29%</b>	-	-	-	<b>55.36%</b>
(a)	0%	7.14%	21.43%	10.71%	0%	0%	25%	9.18%
(b)	7.14%	21.43%	7.14%	7.14%	<b>35.71%</b>	17.86%	7.14%	14.80%
(c)	35.71%	25.00%	28.57%	32.14%	32.14%	35.71%	17.86%	29.59%
Ours	<b>57.14%</b>	<b>46.43%</b>	<b>42.86%</b>	<b>50.00%</b>	32.14%	<b>46.43%</b>	<b>50.00%</b>	<b>46.43%</b>

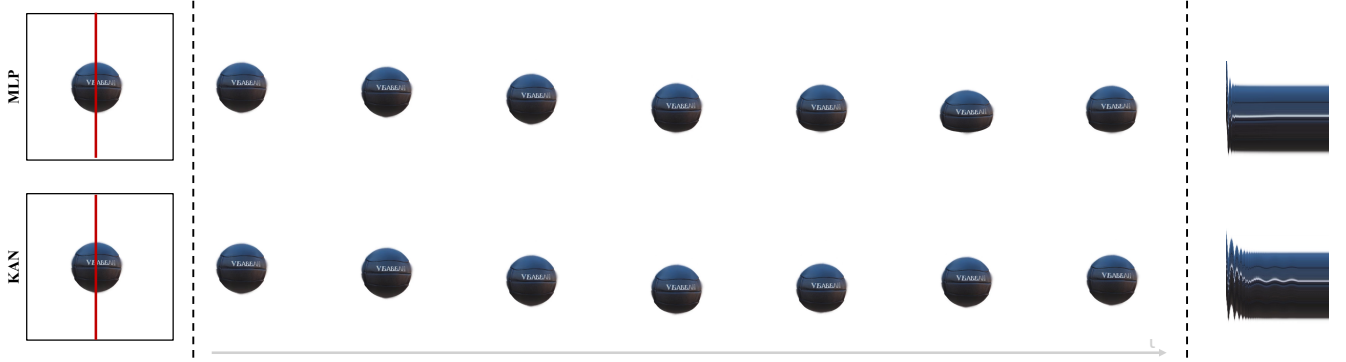


Figure 6: Visualization of ablation study on KAN.

MPM operates through two key phases: Particle-to-Grid (P2G) Transfer and Grid-to-Particle (G2P) Transfer.

**Particle-to-Grid (P2G) Transfer.** In this phase, the mass and momentum of particles are transferred to the grid nodes using interpolation functions. The mass at a grid node  $i$  is computed as:

$$m_i^n = \sum_p w_{ip}^n m_p,$$

where  $m_p$  is the mass of particle  $p$ , and  $w_{ip}^n$  is the interpolation weight (often derived from a B-spline kernel) between particle  $p$  and grid node  $i$ . The momentum at the grid node is similarly updated:

$$m_i^n \mathbf{v}_i^n = \sum_p w_{ip}^n m_p (\mathbf{v}_p^n + \mathbf{C}_p^n (\mathbf{x}_i - \mathbf{x}_p^n)),$$

where  $\mathbf{v}_p^n$  is the velocity of particle  $p$ ,  $\mathbf{C}_p^n$  represents the affine velocity field gradient, and  $\mathbf{x}_i$  and  $\mathbf{x}_p^n$  are the positions of the grid node and particle, respectively.

The grid velocities are then updated based on the external forces and internal stresses computed from the particle data:

$$\mathbf{v}_i^{n+1} = \mathbf{v}_i^n - \frac{\Delta t}{m_i^n} \sum_p \boldsymbol{\tau}_p^n \nabla w_{ip}^n V_p^0 + \Delta t \mathbf{g},$$

where  $\Delta t$  is the time step,  $\boldsymbol{\tau}_p^n$  is the stress tensor of the particle  $p$ ,  $V_p^0$  is the initial volume of the particle, and  $\mathbf{g}$  is the acceleration due to gravity.

**Grid-to-Particle (G2P) Transfer.** After updating the grid, the changes in velocity and momentum are transferred back

to the particles. The velocity of particle  $p$  is updated as:

$$\mathbf{v}_p^{n+1} = \sum_i \mathbf{v}_i^{n+1} w_{ip}^n,$$

and the new position of the particle is given by:

$$\mathbf{x}_p^{n+1} = \mathbf{x}_p^n + \Delta t \mathbf{v}_p^{n+1}.$$

Additionally, the affine velocity field gradient  $\mathbf{C}_p^{n+1}$  and deformation gradient  $\mathbf{F}_p^{n+1}$  are updated as:

$$\mathbf{C}_p^{n+1} = \frac{4}{(\Delta x)^2} \sum_i w_{ip}^n \mathbf{v}_i^{n+1} (\mathbf{x}_i - \mathbf{x}_p^n)^T,$$

$$\mathbf{F}_p^{n+1} = (\mathbf{I} + \Delta t \mathbf{C}_p^{n+1}) \mathbf{F}_p^n.$$

MPM combines the advantages of Lagrangian (particle-based) and Eulerian (grid-based) methods, making it particularly effective for simulating materials that undergo large deformations, fractures, and complex interactions. It has been successfully applied to a variety of materials, including solids, fluids, granular media, and textiles. Moreover, its suitability for parallel computation on GPUs enables high-performance simulations of large-scale problems.

### Score Distillation Sampling

Score Distillation Sampling (SDS) is a core technique introduced in DreamFusion (Poole et al. 2022). The method is a significant advancement in the realm of generating 3D content by 2D diffusion models. Its goal is to create 3D objects that, when rendered from various angles, look like realistic images. Traditional diffusion models are typically used

---

**Algorithm 1: DreamPhysics**


---

```

1: Input: text/image condition  $y$  and static 3D GS scene  $\{\mathcal{G}_i\}$ 
2: Initialize material field  $\phi^{(0)}$  and MPM simulator  $\mathcal{M}$ 
3: Load: video diffusion model  $v$ 
4: while not converged do
5:   ► Step 1: Physics-Based Simulation
6:   Extract physical parameters  $\{\theta_{\mathcal{G}_i}\}$  as  $\theta_{\mathcal{G}_i} = \phi^{(k)}(x_i)$ 
7:   Simulate time status  $\mathcal{M}(\mathcal{G}, \theta) = \{x_i(t), \Sigma_i(t), \Omega_i(t)\}$ 
8:   ► Step 2: Motion Distillation Sampling
9:   Sample viewpoints  $\{c_1, c_2, \dots, c_{MT}\}$  and timestep  $\mu$ 
10:  Render video frames  $\{I_1, I_2, \dots, I_{MT}\}$  and split  $M$  groups of
    videos  $\{V_{\mathbf{r}(t_i)} = [I_i, I_{i+M}, \dots, I_{i+M(T-1)}]\}, i = 1, \dots, M$ 
11:   $\mathbf{s}_{\text{MDS}} = \omega(\mu) (\hat{\epsilon}_v(V_{\mathbf{r}(t_i)}; \mu, y) - \hat{\epsilon}_v(I_i; \mu, y))$ 
12:   $\nabla_{\theta_{\mathcal{G}}} \mathcal{L}_{\text{MDS}}(\theta_{\mathcal{G}}, \mathbf{r}(t_i)) \triangleq \mathbb{E} \left[ \mathbf{s}_{\text{MDS}} \frac{\partial V_{\mathbf{r}(t)}(\theta_{\mathcal{G}})}{\partial x, \Sigma, \Omega} \frac{\partial x, \Sigma, \Omega}{\partial \theta_{\mathcal{G}}} \right]$ 
13:  ► Step 3: Gradient Propagation
14:   $\nabla_{\phi} \mathcal{L}_{\phi}(x, \mathbf{r}(t)) \triangleq \mathbb{E} \left[ \mathcal{L}_{\text{MDS}}(\phi^{(k)}(x), \mathbf{r}(t)) \frac{\partial \theta_{\mathcal{G}}}{\partial \phi} \right]$ 
15:   $\phi^{(k+1)} \leftarrow \phi^{(k)} - \nabla_{\phi} \frac{1}{M} \sum_{i=1}^M \mathcal{L}_{\phi}(x, \mathbf{r}(t_i))$ 
16:  ► Check Convergence
17:  if  $[\phi^{(k+1)}, \phi^{(k)}, \phi^{(k-1)}]$  in same order of magnitude then
18:    converged  $\leftarrow$  True
19:  end if
20: end while
21: return physical parameters  $\theta_{\mathcal{G}_i} = \phi^{(k+1)}(x_i)$ 

```

---

SDS allows the generation of complex 3D structures that, when rendered, produce images consistent with the output of the original 2D diffusion model. This approach significantly broadens the applicability of diffusion models beyond their traditional 2D domain, enabling the efficient creation of detailed and realistic 3D models.

to generate outputs that match the dimensionality of their training data (e.g., 2D images). However, the challenge here is to leverage these models to optimize 3D structures.

To bridge the gap between 2D diffusion models and 3D object creation, DreamFusion uses Differentiable Image Parameterization (DIP). In this approach, a differentiable generator  $g$  transforms a set of parameters  $\theta$  into an image  $\mathbf{x} = g(\theta)$ . For 3D model creation,  $\theta$  represents the parameters of a 3D volume, and  $g$  is a volumetric renderer that generates 2D images from different viewpoints.

SDS optimizes the 3D parameters  $\theta$  so that the generated image  $\mathbf{x} = g(\theta)$  appears like a sample from a pre-trained, frozen diffusion model. The key idea is to bypass the expensive computation of the full diffusion model gradient by simplifying the process.

The gradient used for optimizing  $\theta$  in SDS is derived as:

$$\nabla_{\theta} \mathcal{L}_{\text{SDS}}(\mathbf{x} = g(\theta)) \triangleq \mathbb{E}_{t, \epsilon} \left[ w(t) (\hat{\epsilon}_{2D}(\mathbf{z}_t; y, t) - \epsilon) \frac{\partial \mathbf{x}}{\partial \theta} \right], \quad (9)$$

where:

- $\hat{\epsilon}_{2D}(\mathbf{z}_t; y, t)$  is the predicted noise by the 2D diffusion model at time step  $t$ .
- $\epsilon$  is the actual noise added.
- $\frac{\partial \mathbf{x}}{\partial \theta}$  is the Jacobian of the image with respect to the 3D parameters.

This gradient effectively guides the 3D model parameters to generate images that align more closely with the high-density regions (plausible images) defined by the diffusion model.

SDS is a groundbreaking method that repurposes 2D diffusion models to guide the creation of 3D models. By optimizing a differentiable parameterization of a 3D volume,